Manufacturing structured surface by combining microindentation and ultraprecision cutting

Jiwang Yan *, Akihiro Horikoshi, Tsunemoto Kuriyagawa, Yasunori Fukushima

Department of Mechanical Systems and Design, Graduate School of Engineering, Tohoku University, Aoba 6-6-01, Aramaki, Aoba-ku, Sendai 980-8579, Japan

ARTICLE INFO

ABSTRACT

A manufacturing method for structured surfaces by combining microindentation and ultraprecision cutting was proposed. Firstly, microindentation was performed on metal materials, such as oxygen free copper and electroless-plated nickel, to generate micro dimples with curved cross-sectional profiles. Secondly, material pile-ups formed around the micro dimples during microindentation were removed by ultraprecision cutting using diamond tools. Piezo actuated high-speed repetitive microindentation tests were performed, and effects of indentation depth, indentation load, indentation pitch and indenter vibration on dimple form accuracy and surface property were experimentally investigated. Effects of cutting conditions on pile-up removal behavior were examined in the diamond turning process after indentation.

© 2011 CIRP.

1. Introduction

Structured surfaces are becoming more and more important in advanced industrial technologies [1]. The ability to deterministically alter the topographic structure of a surface can have a profound effect on the surface functions. The mechanical, optical, tribological, and fluidic characteristics, as well as many other properties, can be altered by fabricating textures and micro structures on a flat or curved surface. For example, a micro lens array is a series of miniaturized lenses that formed in a one-dimensional or two-dimensional array on a supporting substrate. The ability of micro lens arrays to focus incident light into a series of beam spots makes them useful in various applications, such as optoelectronic devices for optical communications and parallel image processing [2]. Recently, fabricating micro lens arrays has become a new research focus.

Micro endmilling is a popular method to fabricate micro lens arrays on various kinds of workpiece materials [3–5]. It has been shown that micro endmilling with single crystalline diamond tools can obtain nanometer level surface finish and submicron level form accuracy [6]. However, in micro endmilling there are a few process limitations. One is the low production efficiency and the other is tool wear. Tool wear involves microchippings and gradual recession of cutting edge. Tool wear will seriously decrease the form accuracy and surface quality of the micro lens arrays,

especially when fabricating large-area lens arrays on hard materials.

In this work, a new method for manufacturing structured surfaces by combining microindentation and ultraprecision cutting was proposed. As shown in Fig. 1, firstly, microindentation was performed on a workpiece to obtain micro dimples; then the pile-ups generated around the dimples during microindentation were removed by ultraprecision cutting using diamond tools. A few advantages are expected by introducing the proposed method. Firstly, tool wear is negligibly small, and the process stability is high. Secondly, the time required for generating a large-area structured surface is significantly shorter than that in micro endmilling. Thirdly, new properties of the dimple surface may be generated during microindentation. For example, surface hardness of the dimples might be improved through the work-hardening effect by performing repetitive indentations.

In this paper, to demonstrate the effectiveness of the proposed method, piezo actuated high-speed repetitive indentation tests were performed, and effects of indentation conditions on dimple form accuracy and surface property were investigated. Effects of cutting conditions on pile-up removal behavior were also examined in diamond turning of the indented surfaces.

2. Experimental procedures

2.1. Experimental apparatus

Both indentation and diamond turning were conducted using an ultraprecision lathe (Toyoda AHN-05, JTEKT Corporation, Japan) whose tables can move under 4-axis (XYZB) numerical control at a

---

* Corresponding author. Tel.: +81 227956946.
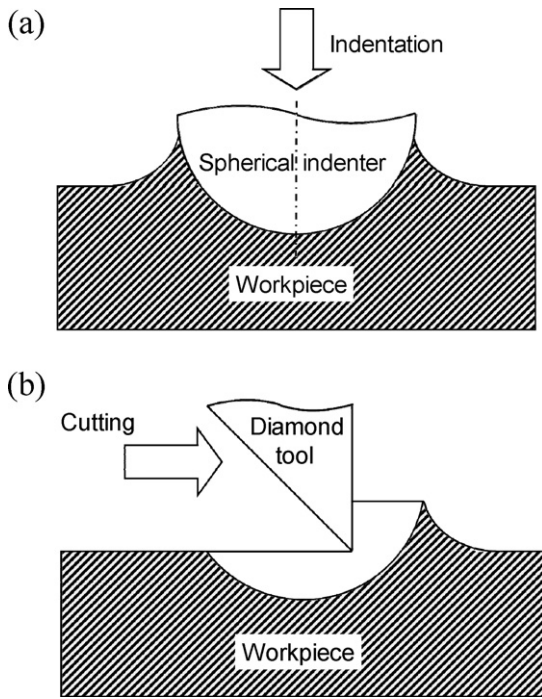 E-mail address: yanjw@pm.mech.tohoku.ac.jp (J. Yan).

(a)

(b)

Fig. 1. Schematic of the process steps.

stepping resolution of 1 nm. To perform high-speed repetitive indentation, we developed a piezo actuator to drive the indenter. The indenter is subjected to a piezo-driven reciprocate movement in the Z direction and a table-driven stepping movement in the X direction. A piezoelectric dynamometer (Kistler 9256A) was mounted below the workpiece to measure the indentation forces. Fig. 2 is a photograph of the main section of the machine.

The piezo actuator is closed-loop controlled by an embedded capacitive sensor at a resolution of 2 nm. The maximum stroke of the actuator is 20 μm and the load capacity is 30 N. The resonant frequency is 2.8 kHz without load and 1.2 kHz at a load of 100 g (0.98 N), respectively. The actuator was controlled by a personal computer through the RS232 interface.

2.2. Indenter and indentation conditions

Spherical type, pyramid type and knife-edge type indenters were used in our research. In this paper, only the results of spherical indenters are given. The radius of the spherical indenters ranges from 10 to 1000 μm. The indenter materials are single crystalline diamond (tip radius 10–100 μm), stainless steel, and tungsten carbide (tip radius 200–1000 μm), respectively. Fig. 3(a) is a scanning electron
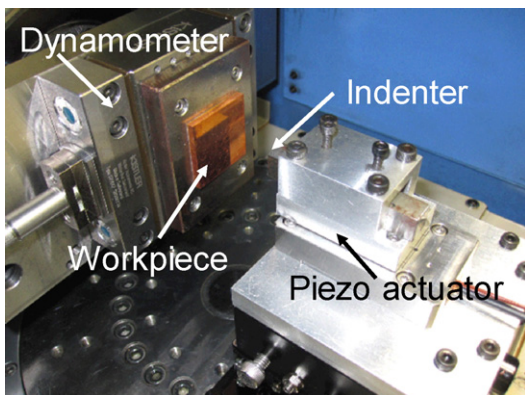

Fig. 2. Photograph of the experimental apparatus.
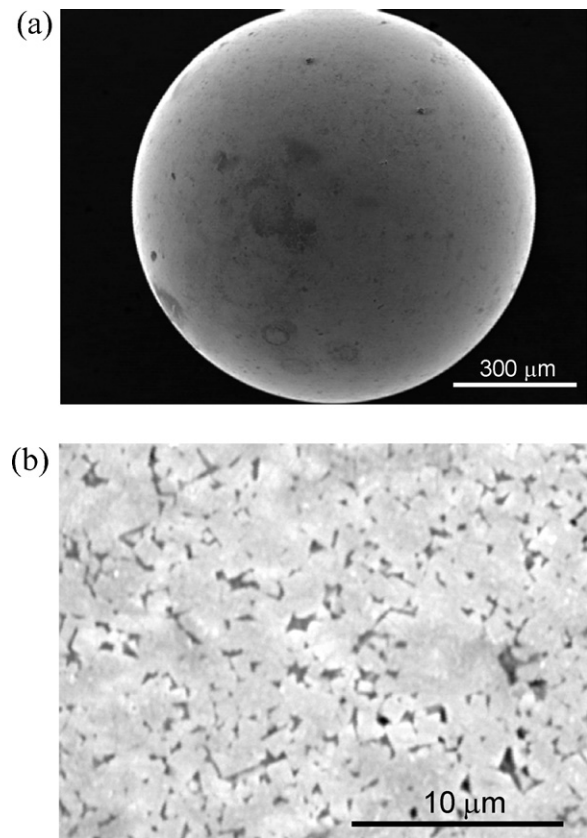
(a)

(b)

Fig. 3. SEM micrographs of a tungsten carbide indenter tip: (a) general view and (b) magnified view.

microscope (SEM) photograph of a tungsten carbide ball which was used as the indenter tip. The roundness tolerance of the indenter tip is within 0.1 μm, and the surface roughness is 155 nmRz and 18 nmRa. Fig. 3(b) is a higher-magnification micrograph of the ball surface. There are many micro pits on the ball surface, which correspond to the grain size of the sintered material.

The workpiece material used in the experiments was oxygen free copper which has a poly-crystalline structure. The workpiece is 30 mm square with a thickness of 5 mm. For comparison, a nickel–phosphorous (Ni–P) electroless-plated steel workpiece, which is another typical mold material, was also used. The plating layer has a thickness of 200 μm and an amorphous structure. To flatten the workpiece surface, the workpiece was face-turned using a diamond tool before the microindentation tests. The surface roughness after diamond turning was $\sim$15 nmRy. The nominal indentation depth, namely, the extension of the piezo actuator, was changed from 5 μm to 20 μm.

2.3. Diamond turning conditions

After indentation, diamond turning experiments were performed using the same ultraprecision lathe to remove the pile-ups generated around the dimples. The workpiece was detached from the dynamometer and chucked onto the air spindle of the lathe through a vacuum chuck.

A single-crystal diamond cutting tool having a nose radius of 0.5 mm was used. The tool rake angle was 0° and the relief angle was 6°. The cutting tool was referenced to the workpiece by the unindented area of the workpiece surface. Depth of cut was set to 1 μm and 2 μm, respectively, and tool feed speed was set to 1 mm/min. The spindle rotation speed was 1000 rpm, and the tool feed per workpiece revolution was 1 μm accordingly. As lubricant and coolant, the Bluebe #LB10 cutting oil was used in the form of mist jet.

3. Indentation results

3.1. Material deformation mechanism

To understand the microscopic deformation mechanism of material in microindentation, dimples indented by a spherical diamond indenter were observed using the SEM. Fig. 4(a) is an SEM micrograph of an indented dimple on the copper workpiece. The dimple surface is very smooth and the dimple fringe is sharp. Around the dimple, material pile-ups have been formed over which numerous slip lines are clearly seen along specific directions. Crystalline boundaries can be seen over the dimple surface and the pile-ups. These phenomena indicate that slipping deformation of the crystal grains dominates the material deformation of copper. For comparison, an SEM micrograph of an indented dimple on the Ni–P workpiece is shown in Fig. 4(b). It can be seen that different from Fig. 4(a), the dimple surface is not smooth but dotted with micro pits. The dimple fringe is wavy and fractured from place to place. The material pile-up has a layered structure, indicating that the pile-up has been formed by material extrusion from under the indenter. Due to the high hardness, existing defects and non-uniformity in material property of the Ni-P plating layer, the surface integrity of the indented dimple is lower than that of copper. In the later sections of the paper, the results of indentation on oxygen free copper will be dealt with.

3.2. Form error

After indentation, the workpiece profile was measured using a laser-probe profilometer NH-3SP (MitakaKouki Co. Ltd.). The laser
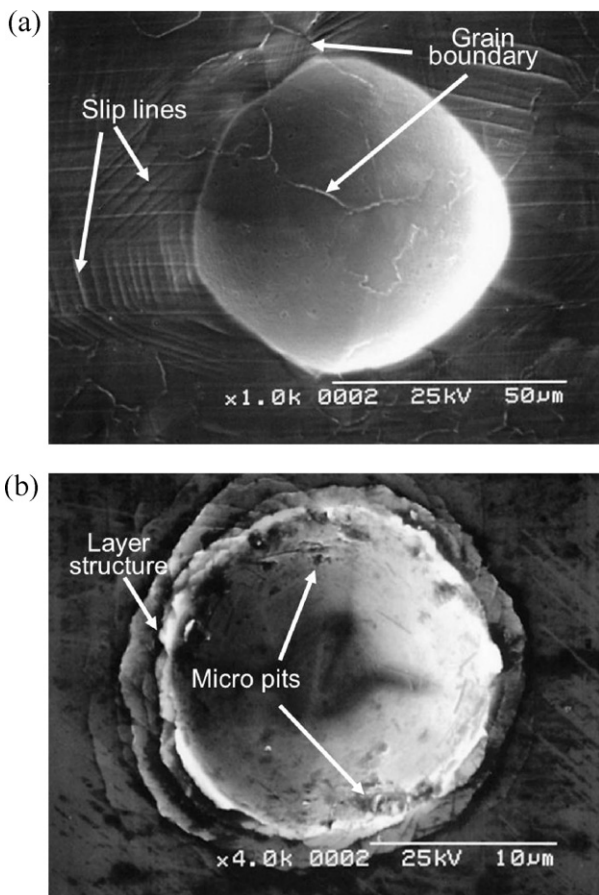

Fig. 4. SEM micrographs of indented dimples on (a) copper and (b) Ni–P plating surface.
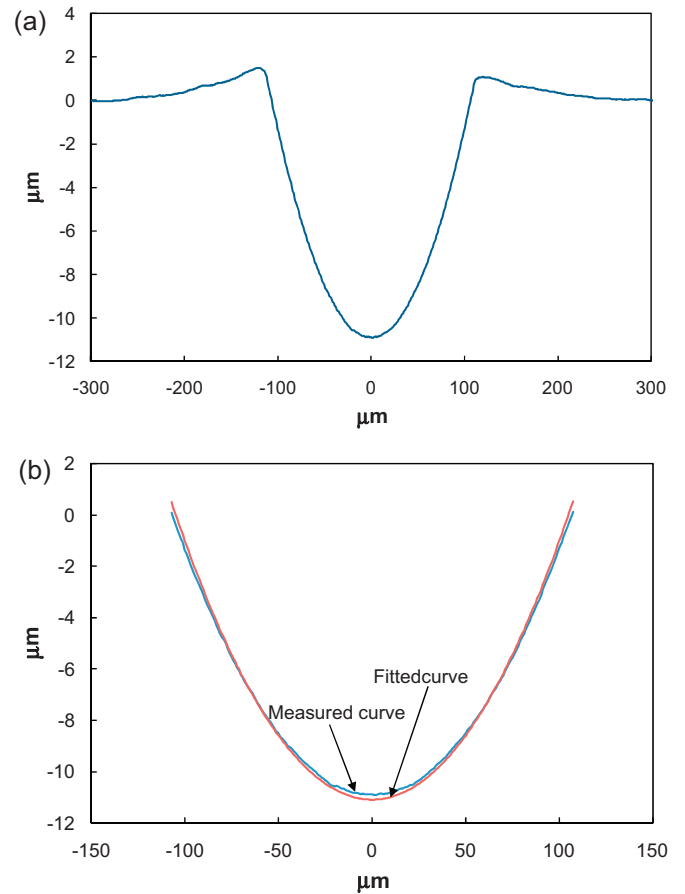

Fig. 5. Cross-sectional profiles of a surface dimple obtained by indentation: (a) general profile and (b) partial profile with comparison with the ideal curve.

beam diameter is extremely small (~1 μm when using a 100× objective lens) and enables measuring the internal surfaces of the small dimples. Fig. 5(a) is a cross-sectional profile of a dimple which was obtained with a tungsten carbide indenter (tip radius 500 μm) after 5 indentations at the same place. The depth of the dimple was 11 μm, remarkably smaller than the nominal indentation depth, namely, 20 μm. The depth error might be caused by the elastic deformation of both the workpiece and the machine elements including the indenter holder and the tool post. On the two sides of the dimple, material pile-ups, the height of which is 1.5 μm, have been generated. Fig. 5(b) is a comparison between the dimple profile (the section below the unindented
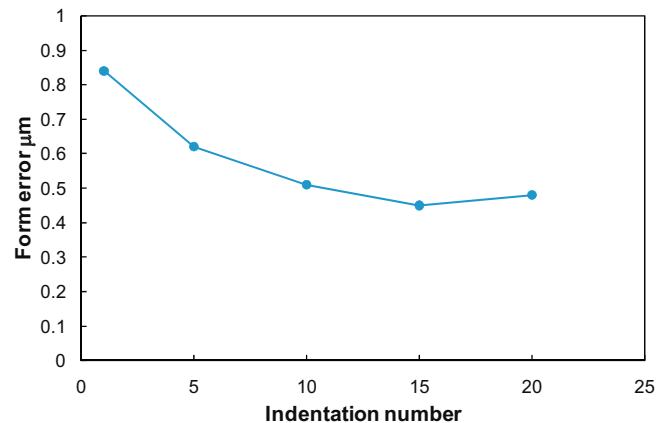

Fig. 6. Change of dimple form error with number of indentations.

surface) and a fitted curve which has the same radius as the indenter (500 μm). The form error of the indent is approximately 0.65 μm. Fig. 6 shows change of dimple form error with number of indentations. The form error decreases with the indentation number. After 15 repetitive indentations, the form error remains almost constant at 0.5 μm. The repetitive indentation might have improved the uniformity of subsurface material plastic deformation, and as a result, reduced the form error of the dimple.

3.3. Surface roughness

Fig. 7(a) and (b) shows SEM micrographs of a dimple and its bottom surface, respectively. The dimple surface is distinctly smoother than the indenter surface (Fig. 3(b)). Fig. 7(c) is a comparison of surface profiles between the indenter and the dimple. The profile was measured using the same laser-probe
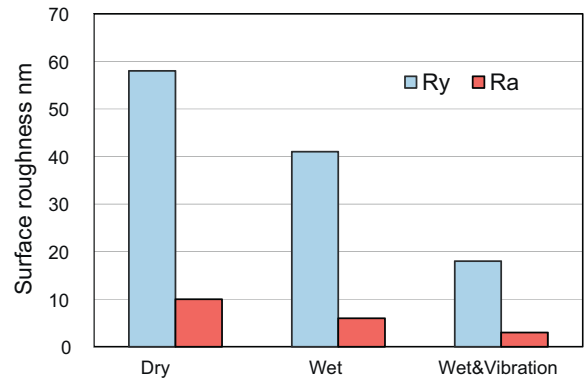

Fig. 8. Comparison of dimple surface roughness obtained in dry indentation, wet indentation, and wet indentation with indenter vibration.

profilometer as that used in Section 3.2. The surface roughness of the dimple is 51 nmRz, about one third of that of the indenter. The micro pits on the indenter surface cannot be completely imprinted into the dimple, leading to a decrease in surface roughness.

To further decrease the surface roughness, it might be effective to reduce the friction between the indenter surface and the workpiece. In this work, we used oil mist (Bluebe #LB10, the same as the coolant for cutting) to lubricate the surface of the indenter and the workpiece during indentation. In addition, to improve lubricating performance, the indenter was vibrated during indentation to assist the lubricant to enter the indenter-workpiece interface. The amplitude and frequency of the indenter vibration were set to 0.25 μm and 75 Hz, respectively. Fig. 8 shows a comparison of dimple surface roughness obtained in dry indentation, wet indentation, and wet indentation with indenter vibration. It is evident that the wet indentation with indenter vibration produces the best surface quality. The surface roughness is 18 nmRy, which is in the same level as the diamond turned surface before indentation (~15 nmRy).

3.4. Surface hardness

The hardness of the dimples was measured before and after indentation using a hardness tester (ENT-1100a, Elionix Co., Ltd., Japan). The hardness tests were made in the middle of the dimples using a micro Vickers indenter. Fig. 9 shows change in the dynamic hardness of the dimples with the number of repetitive indentations. Dynamic hardness is characterized by the indentation
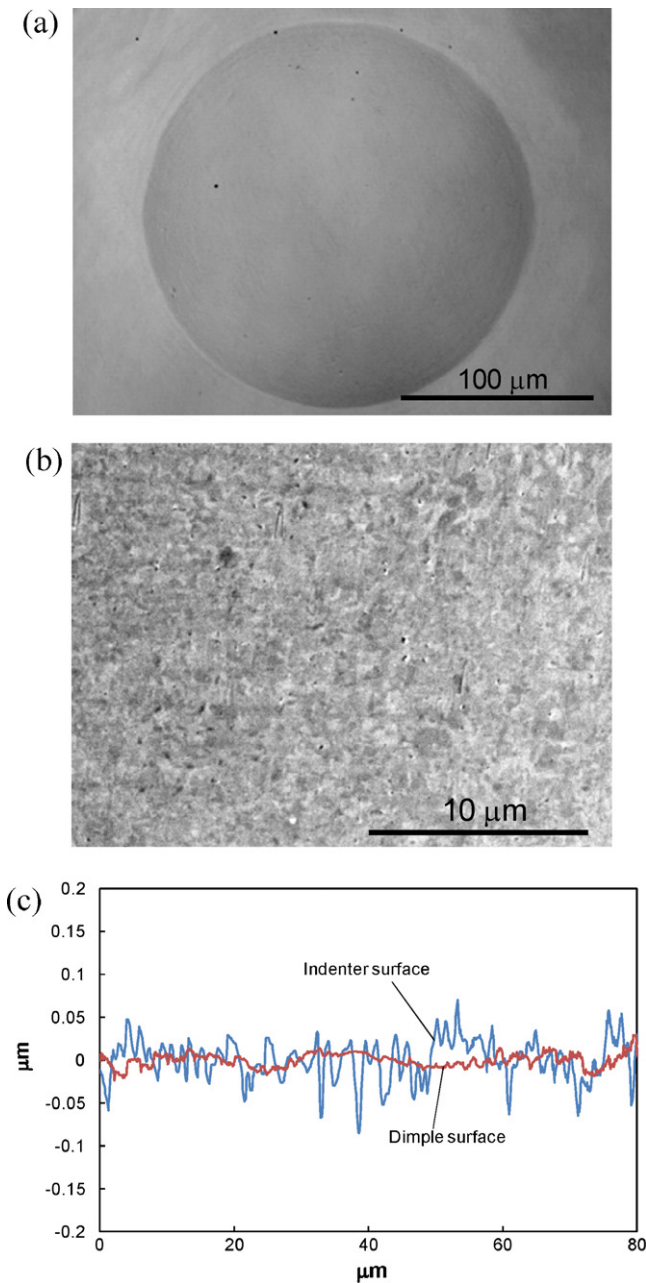

Fig. 7. SEM micrographs of an indented dimple: (a) general view, (b) detailed view of the dimple surface; (c) is a comparison of surface roughness profiles between the indenter and the dimple.
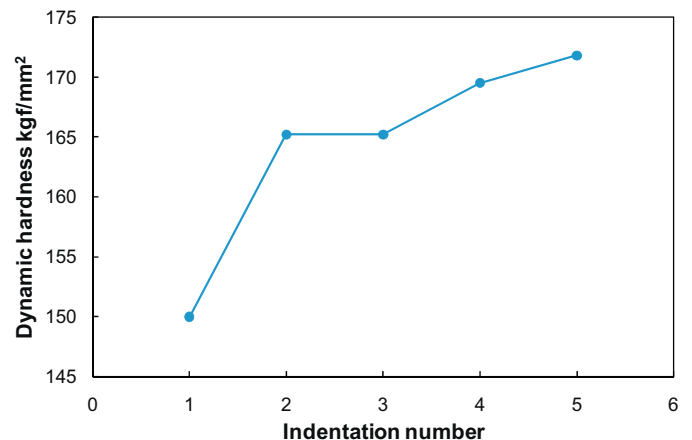

Fig. 9. Change in surface hardness of indented dimples with the number of repetitive indentations.

pressure calculated from the maximum indentation load (100 mN) and the maximum indentation depth. In Fig. 9, we can see that the surface hardness increases sharply for the first two indentations, and keeps increasing gradually as the indentation number further increases.

The increase in surface hardness after indentation might have been caused by the work-hardening effects. Fig. 10 is an example of finite element method (FEM) simulation of the residual strain in the material after indenter unloading. The simulation was performed using a commercially available FEM program MSC-MARC. The yield stress, the Young's modulus, and the Poisson's ratio of the workpiece materials were set to 304 MPa, 1.298×10^5 MPa, and 0.343, respectively. The friction coefficient between the indenter and workpiece was set to 0.1. The indenter was considered as a rigid body without deformation in the simulation.

In Fig. 10, a subsurface deformation layer is clearly seen under the dimple surface. It is the high stain in this layer that caused the work-hardening effects. The surface hardening effect induced by microindentation has many technical advantages. For example, if the indented workpiece is used as a mold for glass molding press or plastic injection molding, the service life of the mold can be improved.

It should be pointed out that, in the simulation model of Fig. 10, for simplicity, we considered the workpiece material as a continuum, and did not care the crystalline orientation effects and grain boundary effects. To precisely simulate the deformation behavior of the polycrystal grains, however, a complicated FEM model which contains multiple grains with different crystalline orientations is needed. This issue is under further investigation.

3.5. Fabrication of dimple array

Fig. 11 shows a plot of recorded indentation force during a single microindentation. From the figure, we can see that the
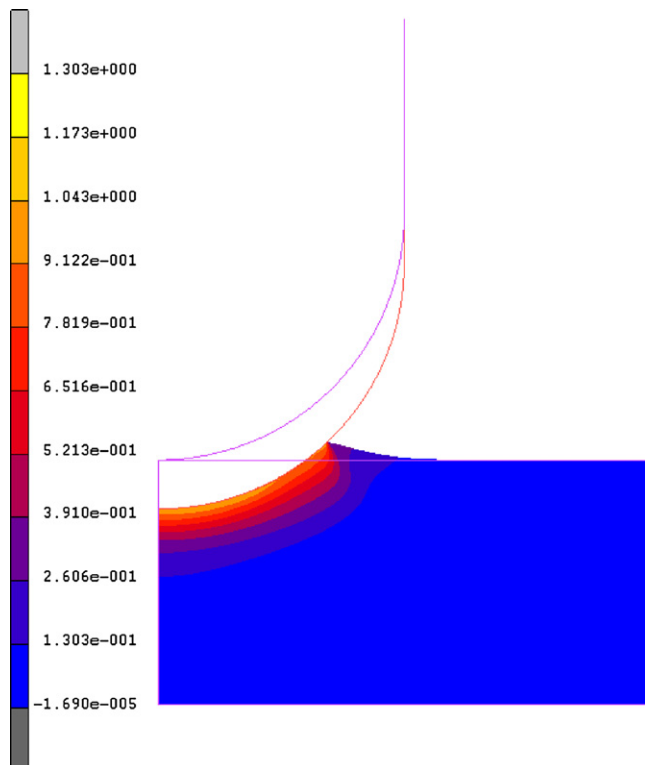

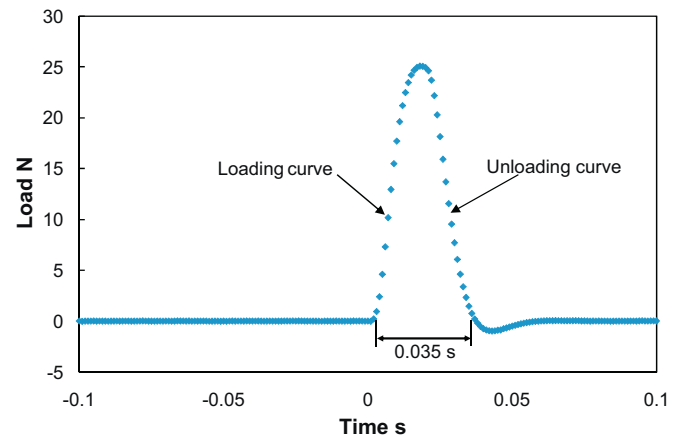**Fig. 10.** FEM simulation of residual strain distribution in the material after unloading.

Fig. 11. Plot of force change during a single indentation.

maximum indentation force is approximately 25 N, and the time for one indentation is 0.035 s. This result demonstrates that piezo-actuated microindentation is effective for high-speed generation of dimple arrays on a large-area surface.

Next, dimple arrays were test fabricated. Fig. 12 shows an optical micrograph of an indented dimple array. The indenter radius used is 500 μm, and the nominal indentation depth is 20 μm, the pitch of the array is 400 μm. It can be seen that the dimples are generally uniform in size. Around the dimples, there are pile-ups of the workpiece material.

Fig. 13(a) is a cross-sectional profile of a dimple array generated at a pitch of 500 μm. It can be seen that he dimples are very uniform in depth. There is no detectable interference among the dimples, and the measured profile agrees very well with the ideal one (the red line). Fig. 13(b) is a cross-sectional profile of a dimple array generated at a pitch of 200 μm. In this case, however, the cross-sectional profile has been severely distorted, indicating interference among the dimples. The critical pitch for dimple interference can be predicted by FEM simulation, which is under further investigation.

4. Diamond turning results

Diamond turning experiments were performed after micro-indentation tests to remove the material pile-ups generated around the dimples. We found that the pile-up removal behavior was sensitive to the depth of cut. Fig. 14 shows SEM micrographs of
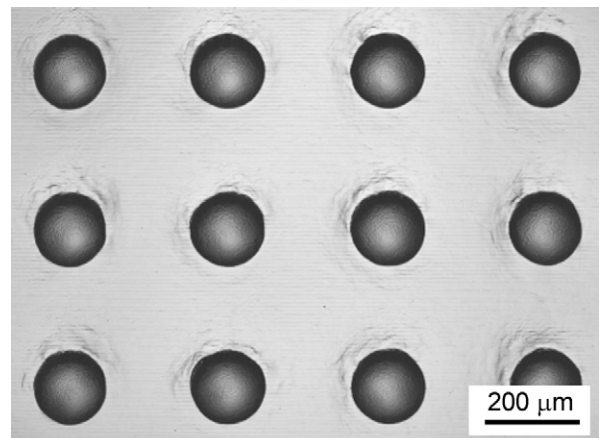

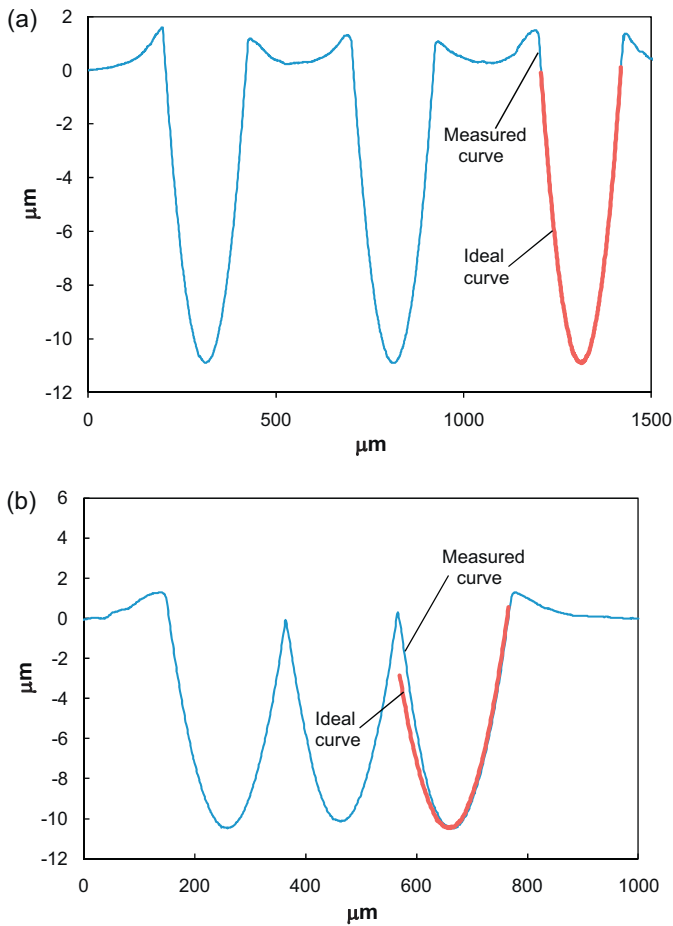**Fig. 12.** Micrograph of a dimple array obtained by microindentation.

(a)

(b)

Fig. 13. Cross-sectional profiles of dimple arrays generated at pitches of (a) 500 μm and (b) 200 μm with comparison with ideal profiles.

Fig. 14. SEM micrographs of indented dimples after diamond turning at different depths of cuts: (a) 2 μm and (b) 1 μm.

two dimples after diamond turning at two different depths of cuts, 1 μm and 2 μm, respectively, at a constant tool feed rate of 1 μm/ rev. At a depth of cut of 2 μm, exit burrs take place significantly around the dimple. In contrast, burr formation around the dimple fringe is greatly suppressed at a depth of cut of 1 μm. The exit burr formation is a result of plastic flow of the workpiece material with high degree of freedom [7]. At the exit of cutting (dimple fringe), there is no constrain to the workpiece material in the direction of cutting, which leads to exit burr formation. As the exit burr is significantly affected by undeformed chip thickness (depth of cut in orthogonal cutting), it is important to use a small depth of cut in diamond turning of the indented surface.

Fig. 15 shows an optical micrograph of a dimple array after diamond turning. The depth of cut used in this case was 1 μm. The size of the dimples has become slightly smaller than that in Fig. 12 due to that the surface layer of material has been removed from the workpiece. In contrast to Fig. 12, no pile-ups of material are seen around the dimples. The burr formation at the dimple fringes is so small that they are hard to identify at this magnification.

Fig. 16 is a higher-magnification SEM micrograph of the fringe of the dimple in Fig. 14(b). Micron-level material protrusion can be clearly seen at the dimple fringe. The formation of material protrusion is related to the cutting force. The bigger the cutting force is, the deeper the subsurface deformation is.

Based on these results, we may say that it is important to decrease the cutting force to suppress the subsurface material deformation. To use a small depth of cut is an effective method to reduce cutting force and eliminate burr formation and subsurface material deformation. The other approach might be to use an
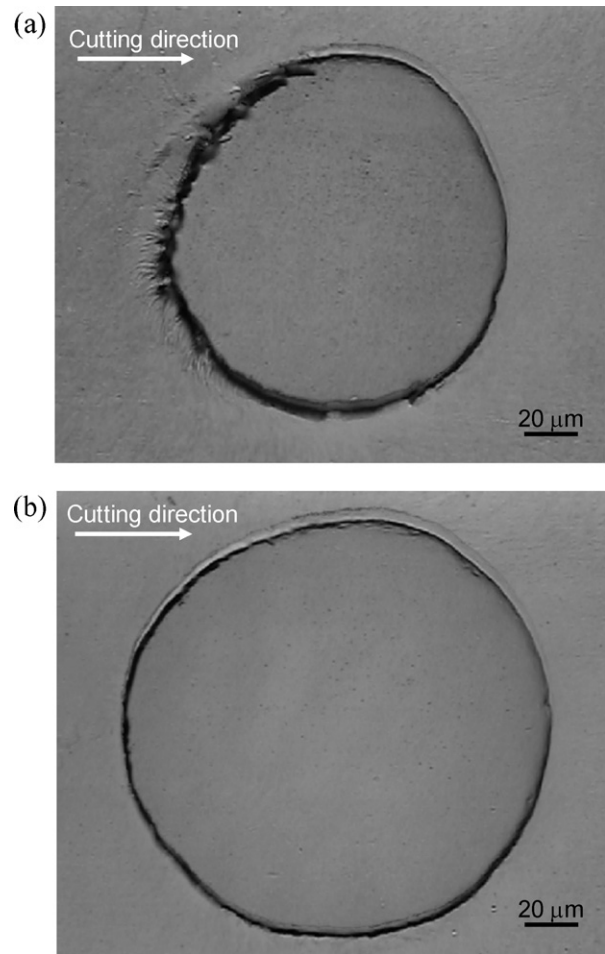
extremely sharpened tool. It should be mentioned that the tool used in the present preliminary experiments was not a new one. Before cutting experiments, we examined the tool using an atomic force microscope and the edge radius of the tool was estimated to be around 200 nm. This tool edge radius is larger than that of a newly sharpened tool, the edge radius of which ranges from a few nanometers to a few tens of nanometers (~50 nm) [8]. Therefore, it is presumable that the bluntness of the cutting tool has contributed to the burr formation shown in Fig. 16. Therefore,
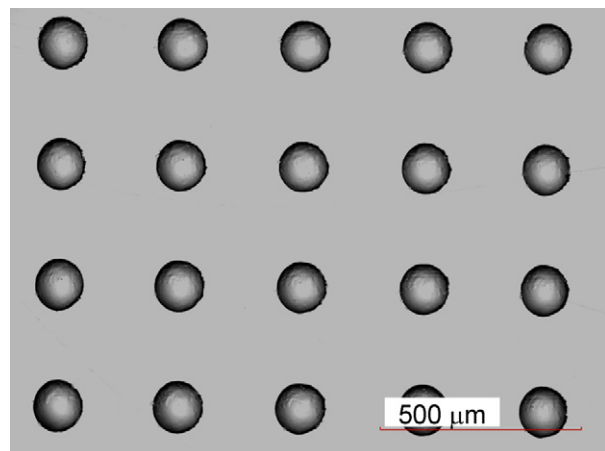

Fig. 15. Micrograph of a part of an indented dimple array after diamond turning.
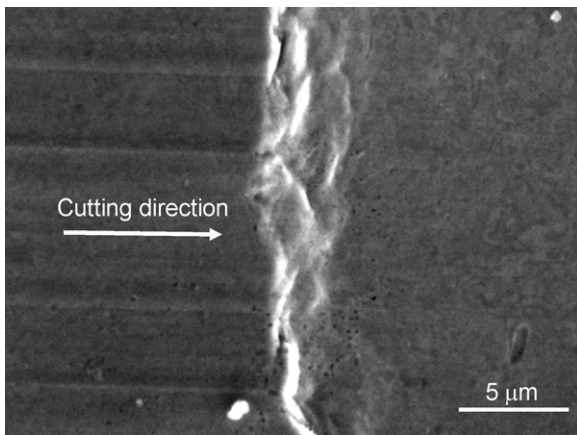
Fig. 16. SEM micrograph of the fringe of the dimple shown in Fig. 14(b).

by using an extremely sharpened diamond tool (for example, edge radius ~10 nm) prepared by fine polishing techniques or non-traditional methods such as ion milling, the burr formation around the dimple edge might be significantly suppressed. This issue is under further investigation.

5. Conclusions

A new method for manufacturing large-area structured surfaces by combining microindentation and ultraprecision cutting was proposed. Piezo actuated high-speed repetitive microindentation was performed and effects of indentation conditions on dimple form accuracy and surface property were experimentally investigated. It was found that the microscopic deformation mechanism depends strongly on the material property. Repetitive indentation can significantly improve the form accuracy of the indented dimples. The surface roughness of the dimples is better than that of the indenter, and oil mist lubrication with indenter vibration is effective to improve the surface quality. The indented surface has a significantly higher hardness than that of the unindented surface. These surface characteristics are useful for improving the service life and anti-wear performance of the fabricated workpiece when it is used as a mold in glass molding or plastic injection molding applications. The effects of cutting conditions, namely, the depth of cut and tool sharpness, on pile-up removal behavior were also examined and discussed in the diamond turning process of the indented surfaces.

References

[1] Evans, C., Bryan, J., 1999, Structured, Textured or Engineered Surfaces, CIRP Annals, 48/2: 541–556.
[2] Lim, C., Hong, M., Lin, Y., Chen, G., Kumar, A., Rahman, M., Tan, L., Fuh, J., Lim, G., 2007, Sub-micron Surface Patterning by Laser Irradiation Through Microlens Arrays, Journal of Materials Processing Technology, 192-193:328–333.
[3] Weule, H., Hüntrup, V., Tritschler, H., 2001, Micro-cutting of Steel to Meet New Requirements in Miniaturization, CIRP Annals, 50/1: 61–64.
[4] Kim, J., Kang, Y., 1997, High-spend Machining of Aluminium Using Diamond Endmills, International Journal of Machine Tools & Manufacture, 37:1155–1165.
[5] Torres, C., Heaney, P., Sumant, A., Hamilton, M., Carpick, R., Pfefferkorn, F., 2009, Analyzing the Performance of Diamond-coated Micro End Mills, International Journal of Machine Tools & Manufacture, 49:599–612.
[6] Yan, J., Zhang, Z., Kuriyagawa, T., Gonda, Y., 2010, Fabricating Micro-structured Surface by Using Single-crystalline Diamond Endmill, International Journal of Advanced Manufacturing Technology, 51/9-12: 957–964.
[7] Nakayama, K., Arai, M., 1987, Burr Formation in Metal Cutting, CIRP Annals, 36/1: 33–36.
[8] Asai, S., Taguchi, Y., Horio, K., Kasai, T., Kobayashi, A., 1990, Measuring the Very Small Cutting Edge Radius for a Diamond Tool Using a New Kind of SEM Having Two Detectors, CIRP Annals, 39/1: 85–88.